Paper ID ICLASS06-277
EXPERIMENTAL INVESTIGATIONS OF A LOW WEBER LIQUID SPRAY IN AIR CROSS FLOW

Pontus Eriksson [1] **Raik Orbay** [2] **Jens Klingmann** [3]

[1]Senior Engineer, Volvo Aero Corporation, pontus.eriksson@volvo.com
[2]Graduate Student, Department of Energy Sciences, Lund University, Sweden, raik.orbay@vok.lth.se
[3] Associate Professor, Department of Energy Sciences, Lund University, Sweden, jens.klingmann@vok.lth.

ABSTRACT A Low Weber water spray subjected to an air cross flow has been investigated. The spray is characterized by low liquid injection velocity, producing a column that is broken up by aerodynamic forces from the oncoming air. PIV and PDA have been used to quantify both the continuous and dispersed phases. Long range microscopy has been used to characterize the column breakup process. It has been shown that bubbles (akin to droplet bag breakup) may form already in the column.

Keywords: Liquid Atomization, Droplet, Liquid Jet in Cross Flow, Low Weber Number, We, Bag Breakup, Bubble

1. INTRODUCTION

Spray behavior under different boundary conditions are of interest for various applications such as aeronautical and industrial gas turbine combustion chambers, military afterburners, crop dusting, greenhouse humidification, chemical engineering, fire protection and pharmaceutics. The particular case where a liquid jet is injected at right angles to a gas flow can be encountered in many instances.

CFD modelers seek high quality data in order to validate spray codes. Therefore, access to accurate measurements of two-phase flows is valuable.

As indicated by Gosh et al. [1] and Birouk et al. [2], the way in which fluid jets are deflected and deformed by cross flows is a fundamental issue in fluid mechanics which is still not fully understood.

This paper reports quantification and visualization of the breakup process and droplet characteristics for a We=15 spray with low liquid injection pressure and no nozzle atomization. This kind of spray is not usually found in technical applications where a well distributed and finely dispersed spray is often desired. Injectors will however, in some cases outside the design envelope, operate under such conditions.

Several mechanisms may interact to transform the continuous liquid phase into droplets. Each mechanism requires a certain timescale in order to have a marked effect on the column morphology. Certain mechanisms may therefore be dominant at various conditions. Breakup may result from internal turbulence, ‘surface shape’ related air pressure variations and forces due to surface tension. The latter will tend to transform the cylindrical column into spherical droplets (Rayleigh breakup). All these mechanisms tend to be significant at low We numbers and would all be expected to play a role in this paper.

At higher We numbers droplets may be stripped off the column sides.

At high injection pressures column breakup may be initiated very near to the injection point and thus preempt other mechanisms.

A comparison between a low We and a high We sprays can be seen in Figure 1. The images are of sprays with similar liquid to air momentum ratios. It can be seen that the low We spray exhibits much larger structures and that the initial resistance from the air on the liquid phase is much less, thus the two sprays will have different initial trajectories.

There are several earlier publications on experimental research of sprays in cross flow, most of which concentrate on higher We number sprays since they are of greater technical importance. Rachner et al. [3] for instance, investigate penetration and atomization of a plain jet of kerosene fuel at conditions relevant to Lean Premixed Prevaporized combustors. Cavaliere et al. [4] also studied sprays at elevated pressures typical of Lean Premixed Prevaporized injectors while Johnson et al. [5] studied sprays under jet engine afterburner conditions. Gosh et al. [1] have developed analytical models for sprays under conditions typical for crop dusting.

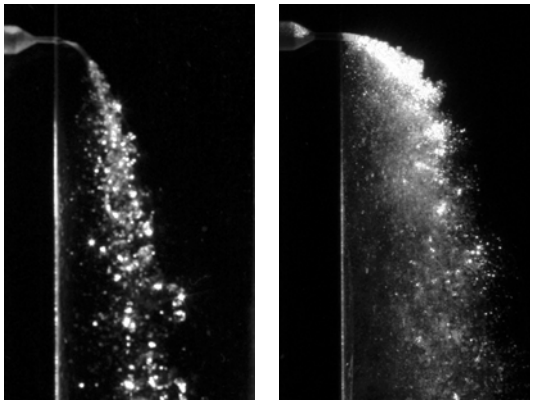

Figure 1: Low We spray (left) and high We spray (right)

2. MATERIALS AND METHODS

An experimental rig (Figure 2) has been devised to allow for optical access from four sides to a rectangular quartz tube (SPECTROSIL 2000) of dimensions in accordance with Figure 3. The rig provides air at pressures up to 1250 kPa and temperatures up to 420°C at the inlet.

At one of the short sides of the tube there is an admission hole for water in the form of an open ended tube

Ø0,46 mm with a L/D=2,4. Demineralized water at pressures up to 8 MPa and temperatures up to 200°C may be injected through this hole. The rig is capable of delivering up to 40 g/s of air mass flow. The dimensions of the test section were chosen to correspond to a lean combustion premix duct, typical of a 5 MW industrial gas turbine.

A Dantec Phase Doppler Analyzer (PDA) system, which provides two velocity components and the particle diameter for each validated droplet/particle, was used to characterize the spray.

The various components of the PDA system were:

- Spectra-Physics Stabilite 2017 Ar/Kr-Ion Laser
- 60X41 transmitter (488 nm and 514,5 nm)
- 60X61 probe
- 57X10 receiving optics
- 58N50 PDA Processor
- Lightweight Traverse
- BSA Flow Software v. 2.12

A Dantec Particle Imaging Velocity (PIV) system was used to characterize air and spray velocity fields.

The PIV system consisted of the following components:

- Big Sky CFR 200 Nd:YAG Laser (532 nm)
- Quantel Big Sky EC CFR 2K Q-switched controllers
- HighSense 80C60 CCD camera
- FlowMap PIV Software v. 3.62

The air velocity field was characterized with Aerosil 200 (SiO_2) with the following characteristics:

- 12 nm average primary particle size, agglomerated to some microns
- tapped density of 50 g/l

A LaVision solid particle seeder; Particle Blaster 100 was used to inject the seeding particles upstream of the test section.

The following imaging equipment was used:

- Nikon D70s digital SLR camera (6.1 MP)
- Questar QM-1 long range microscope with 2x Barlow lens (diffraction limit down to 3μm)
- Nikon Micro-Nikkor 60 mm f/2.8D macro lens

The investigated spray conditions were in accordance with Table 1 unless otherwise specified. At the injection point the We number was kept at 14.6 and the liquid to air momentum ratio q was 21.

Table 1

	Air	Water	Unit
Inlet temperature	25	25	°C
Pressure	200	~200	kPa
Massflow	8	1.12	g/s
Bulk velocity	30.4	6.7	m/s
Reynolds number	35300	3100	-

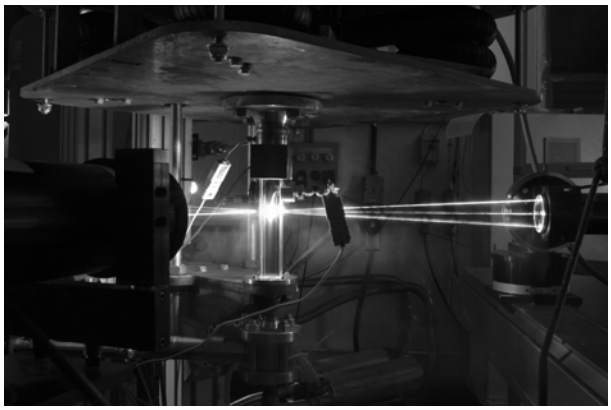

Figure 2: Test rig

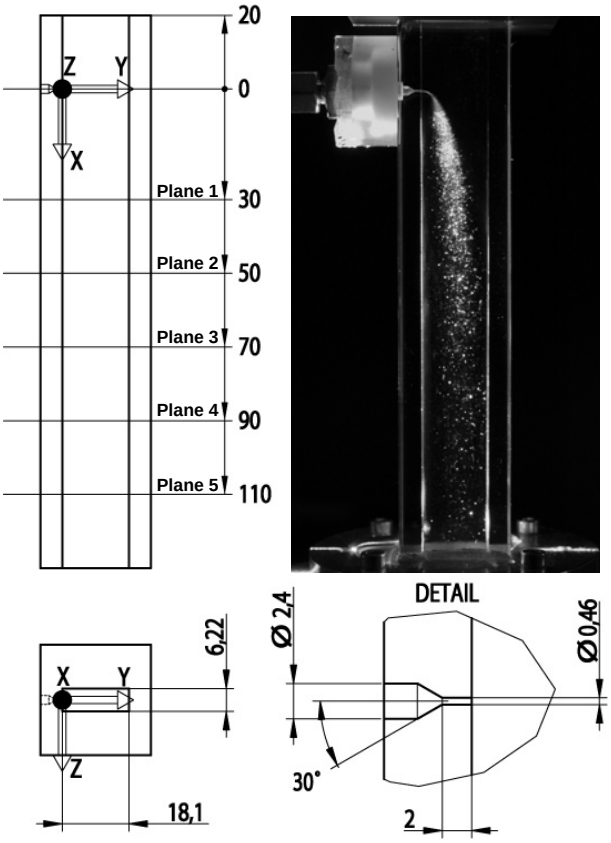

Figure 3: Test section, dimensions in mm

Air and spray flow field velocity characterizations were performed with the PIV system and the 60 mm macro lens.

The air velocity field was characterized without the presence of a spray. For the air velocity field the time between laser pulses was 10 μs. A 16x16 pixel size interrogation area with a 25% overlap was specified. Peak validation was performed with a peak height ratio of 1.2.

For the spray visualization the time between laser pulses was 18 μs. A 64x64 pixel size interrogation area with a 25% overlap was specified. Peak validation was again performed with a peak height ratio of 1.2.

The spray flow field was characterized with the PDA system at the five planes shown in Figure 3. The system was set up to admit the beam system through the wall containing the injection hole. The emitting probe centerline was aligned with the liquid injection direction.

The receiving probe was oriented to receive scattered light in first order refraction at the Brewster angle (73.7° off-axis in scatter plane). Parallel polarization was selected. The measurement volume size was approximately 0.2 mm in diameter. All PDA data was recorded at Z=0. U velocities for each validated droplet and associated diameter information was recorded. In each plane 15 points (distributed in the Y direction) were scanned. Generally 5000 samples were recorded. In regions with a low droplet count, the sampling time was limited to 10 minutes.

One of the Big Sky CFR 200 lasers was used as an illumination source for the photographic imaging of the spray. The laser sheet was aligned with the Z=0 plane and defocused in order to illuminate the entire spray. The Q-switch was adjusted in the range 140 – 200 μs to yield proper exposure times. A laser pulse rate of 4 Hz and an exposure time of 1/4 s on the Nikon D70s yielded one image per exposure.

3. RESULTS

The entire test section air velocity field was mapped (without spray) at Z=0. This is shown in Figure 4. The figure also shows the spray velocity field near the injection point. It can be seen that the air velocity field in the mid plane (Z=0) increases with X. This is attributed to the growth of boundary layers at the walls. At the inlet the velocity is close to the bulk inlet velocity (30.4 m/s) indicating that boundary layers are thin.

Figure 4 also shows the spray velocity field near the injection point. The spray is accelerated rapidly by the high relative velocity. It can also be seen that droplet velocities decrease with increasing Y. This is attributed to the fact that larger structures of the spray have higher inertia and therefore penetrate further in the Y direction. These structures are subsequently accelerated less readily by the air flow in the X direction. Since the spray is seen to accelerate fast in the initial 18 mm of the test section, droplet We numbers are expected to drop to stable values well above plane 1.

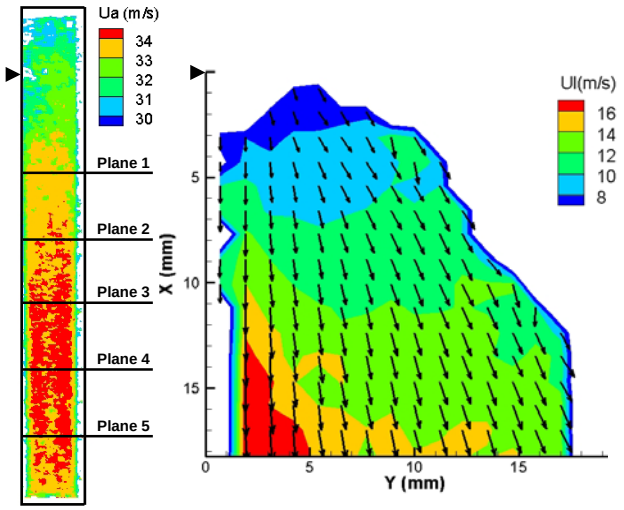

Figure 4: PIV air velocity field (left) and spray velocity field (right), Z=0

Figure 5 shows the spray at nominal conditions but with a minimal amount of air flow in order to keep the quartz wall between the camera and the spray clean from water.

With the much reduced aerodynamic forces on the column, surface structures stemming from the injection process can be seen. A short compact zone (approximately 1 hole diameter long) is followed by a wrinkled column which stays intact all the way up to the opposite wall at Y=18.1 mm.

The Reynolds number for the liquid is close to the transition point between laminar and turbulent pipe flow. This will affect the behavior of the injected column. Figure 6 and Figure 7 are both showing nominal conditions (within reasonable tolerances) but still differ substantially from the typically observed morphology (Figure 8 and Figure 9). The spray in Figure 6 is branching into an upper and a lower sub-column. On average, the trajectory is however consistent with the typically observed spray, reflecting an overall conserved change of momentum in the X direction.

A long laminar compact zone is seen in Figure 7. This column has not transitioned to the turbulent flow that can be seen in Figure 5. Figure 7 also shows a spiraling flow which may be associated with von Karman vortex shedding.

In Figure 8 surface waves are seen to grow and turn into protuberances, which further disintegrate into ligaments and droplets. These kinds of structures, together with satellite droplet formation may be seen in Figure 9.

Premature droplets may form very close to the injection point. This may be attributed to imperfections in the orifice. An example of such behavior is shown in Figure 10.

In Figure 11, Figure 12 and Figure 13 examples of column bubble formation and disintegration can be seen. Very small droplets (in the order of 10 μm) are formed from the disrupted membrane. The bubbles are formed when an indentation on the windward side of the column is subjected to an elevated stagnation pressure. This will exacerbate the process of forming a cavity in the column, which will turn into a bubble. This phenomenon is quite similar to bag breakup of droplets.

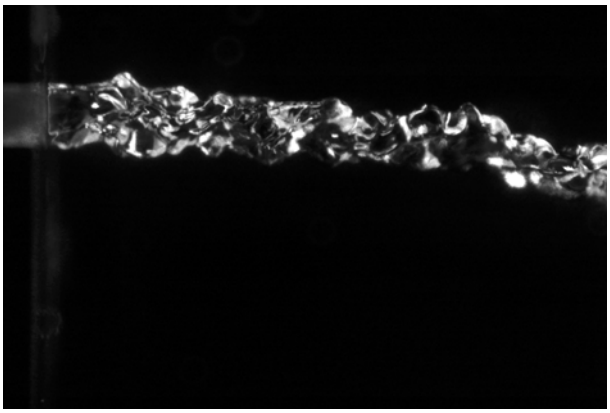

Figure 5: 3.8 g/s air flow

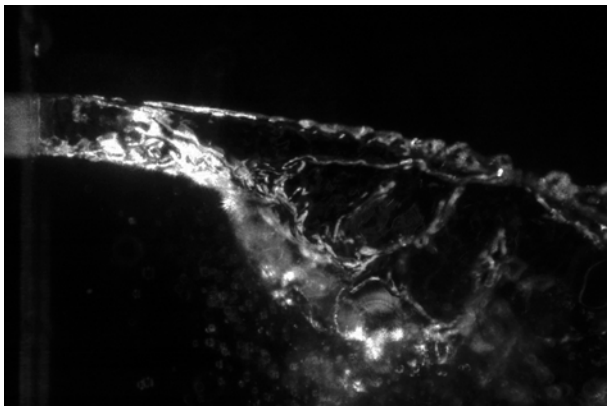

Figure 6: Branching efflux

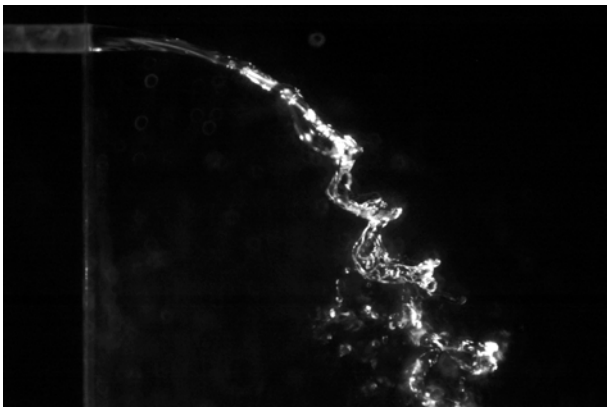

Figure 7: Spiral efflux

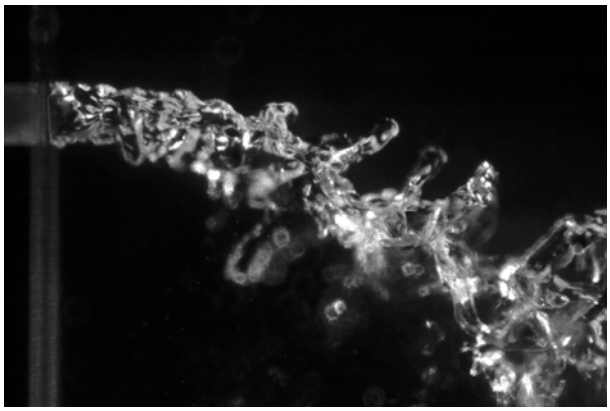

Figure 8: Protuberance structures

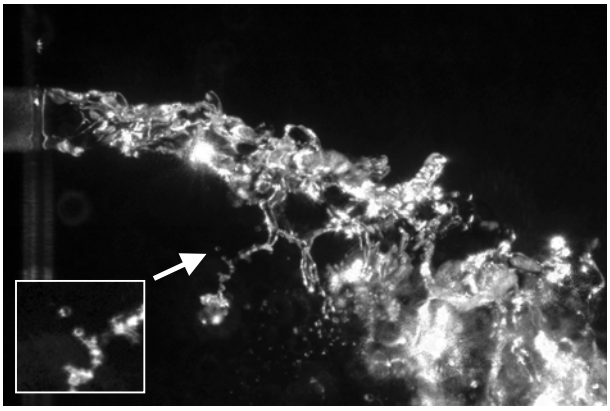

Figure 9: Ligaments forming large and small droplets

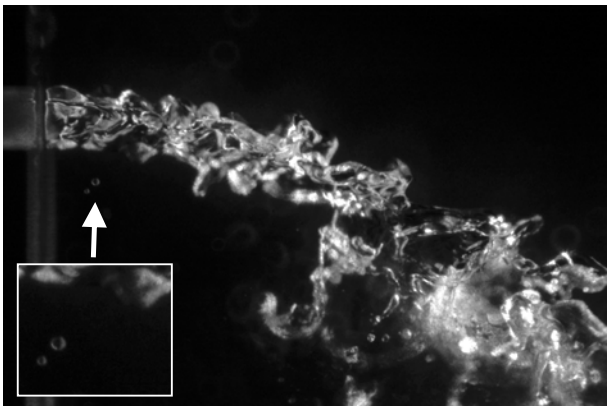

Figure 10: Early droplets

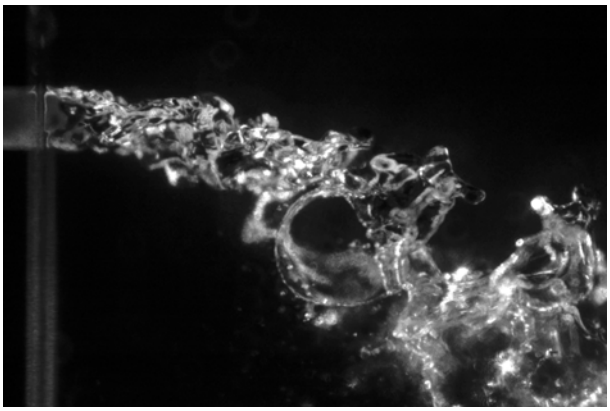

Figure 11: Bubble forming, 1.2 g/s water flow

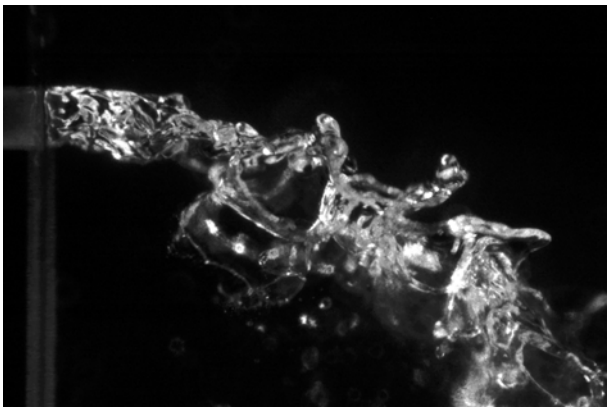

Figure 12: Bursting bubble

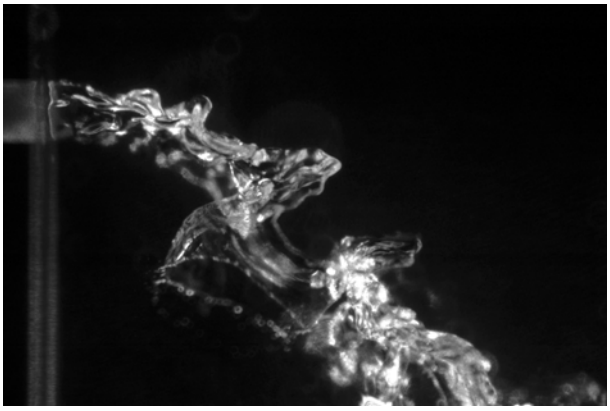

Figure 13: Bursting bubble, 0.8 g/s water flow

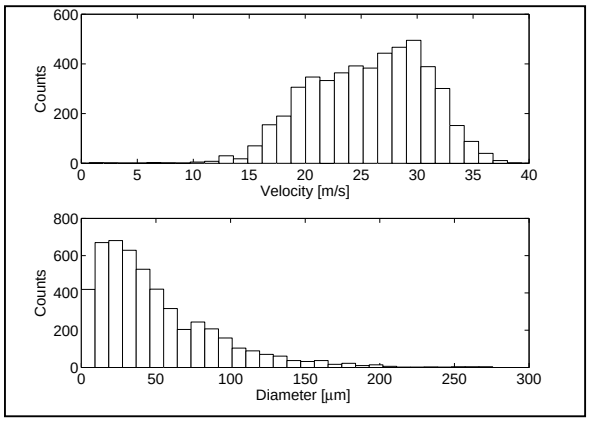

Figure 14: PDA droplet histograms, X=70, Y=9.05, Z=0

Figure 14 shows a typical set of velocity and diameter probability density functions for a point in the spray.

As seen in Figure 15 through Figure 19, the general trends for mean droplet diameters are increasing in the positive Y direction. This again shows that larger structures penetrate further. At plane 5 however, a more uniform distribution is observed.

The planewise averaged D[1,0] and D[3,2] are not changing between plane 1 and 5. D[1,0] is 55 µm and D[3,2] is 110 µm. It is concluded that the entire break up process therefore has already occurred before plane 1. Any change in diameter and velocity spectra between planes is therefore dominated by spatial redistribution of intact droplets.

In the middle regions, where the spray core is blocking the air flow, droplet velocities are lower due to less availability of aerodynamic force. Continuity will in turn dictate a higher air velocity outside the spray core. This will tend to increase aerodynamic force on the droplets outside the core and accelerate entrained droplets.

As was observed in the diameter plots (Figure 15 – Figure 19), a more uniform velocity distribution is observed for plane 5.

An empirical correlation for average droplet sizes is given by Bayvel et al. [6]:

for $\mathrm{We}\,\mathrm{Re} < 1e6$

$$D[3,2] = 3.9D(\mathrm{We}\,\mathrm{Re})^{-0.25}$$

According to this equation D[3,2] will be 82 µm. The spray conditions forming the basis for this formula were however possibly quite different and in all likelihood more akin to technical sprays.

Figure 20 also shows the relationship between droplet size and velocity. The larger droplets exhibit slower velocities. The 2nd order curvefits are shown on top of the data set for plane 2 at Y=9.05 and Z=0 (with the scatter around the curves at low velocities being quite large). The velocity-size relationship seems to be fully established in plane 4 since the curve fits are essentially the same for the last two planes.

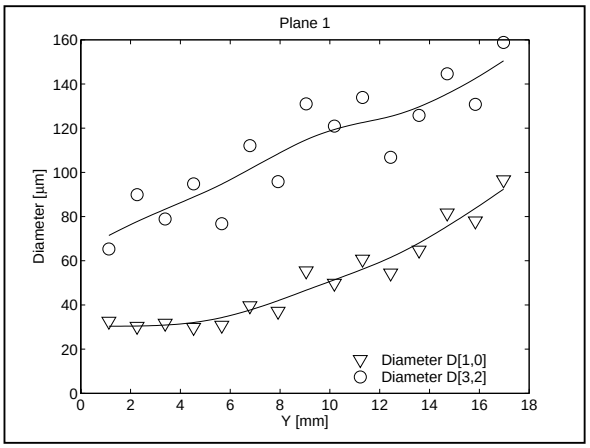

Figure 15: PDA Mean droplet diameters, Z=0

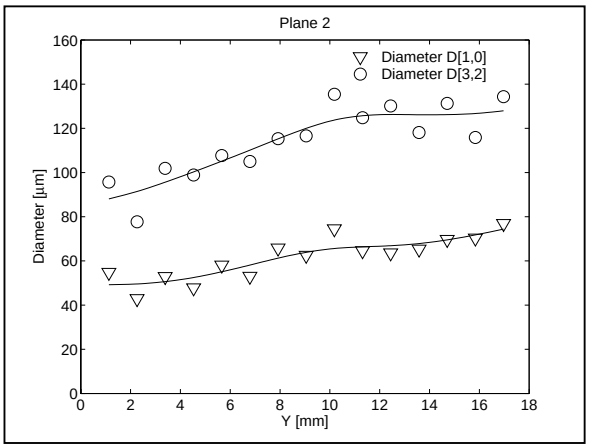

Figure 16: PDA Mean droplet diameters, Z=0

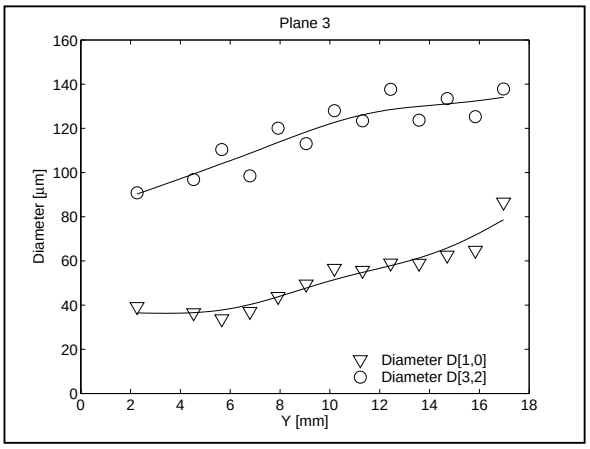

Figure 17: PDA Mean droplet diameters, Z=0

Figure 21 and Figure 22 show velocity information for each of planes 1 – 5. The general trend is that droplet velocities drop off with increasing Y coordinate value, to about Y=9 mm, where after they increase.

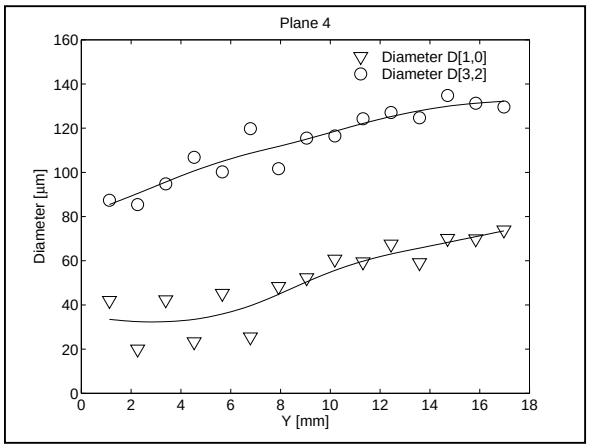

Figure 18: PDA Mean droplet diameters, Z=0

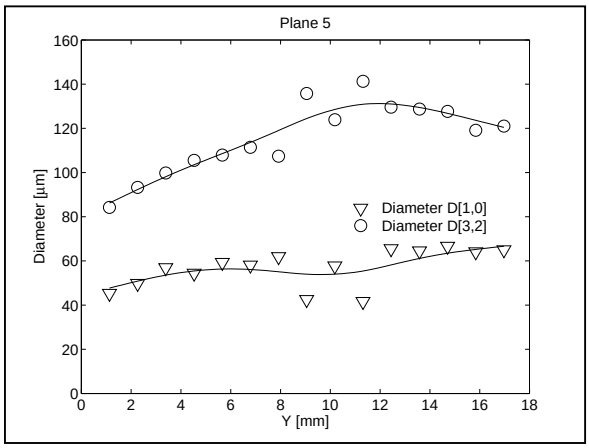

Figure 19: PDA Mean droplet diameters, Z=0

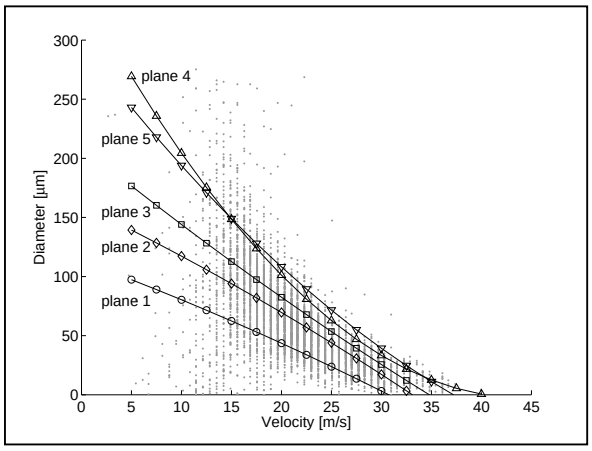

Figure 20: PDA 2D PDF of spray, Y=9.05, Z=0

In Figure 22 the presence of droplets affect the turbulence characteristics of the flow field. A slight increase of RMS values can be observed where the core is present.

Figure 23 shows the development of U velocity and its fluctuations as the spray progresses through the test section. The spray velocity is seen to be approaching the bulk velocity asymptotically while the RMS velocity is largely unaffected.

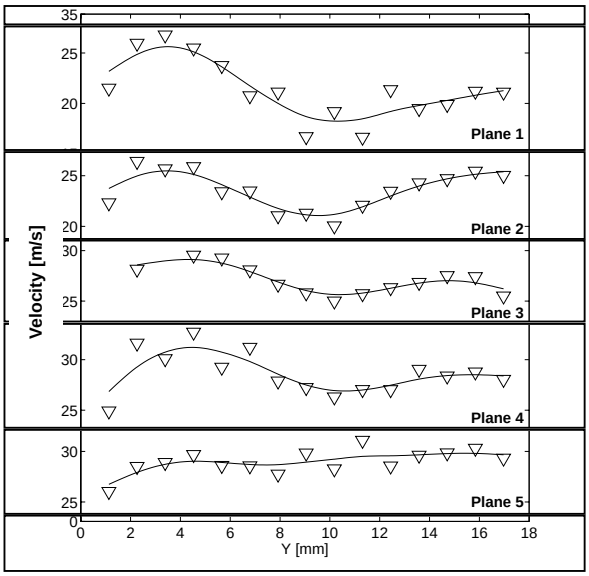

Figure 21: PDA droplet velocity profiles, Z=0

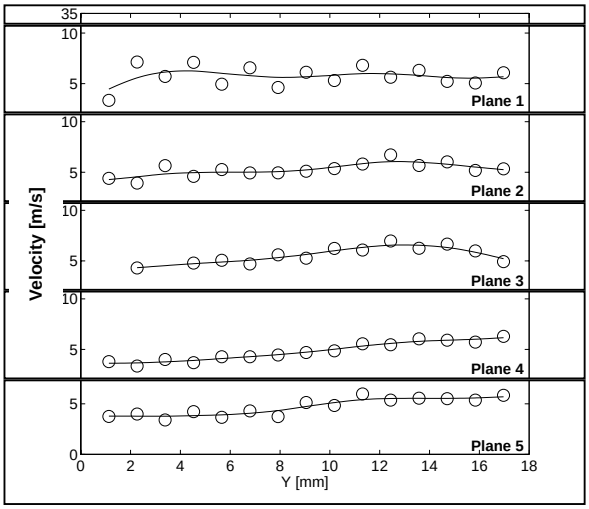

Figure 22: PDA droplet RMS velocity profiles, Z=0

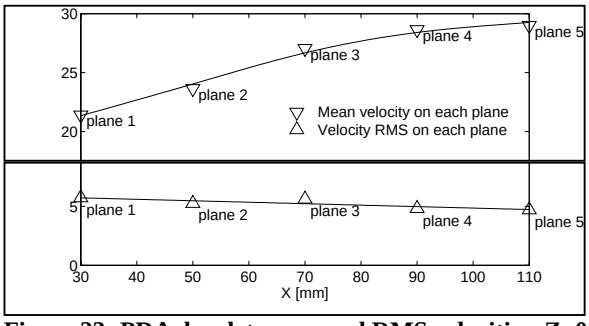

Figure 23: PDA droplet mean and RMS velocities, Z=0

4. CONCLUSION

A low We water spray has been investigated.

A long range microscope has been used to image the breakup process. Velocity fields, both from the continuous and dispersed phase have been measured with PIV and PDA.

The breakup is solely caused by the impinging air impacting on the buckled column. Breakup has already finished before plane 1, since droplet We numbers rapidly drop to stable values.

Imaging shows that different flow regimes exist due to slight variations in geometry and flow conditions.

A complex mix of different breakup mechanisms leads to the formation of a spray. Surface buckling due to internal turbulence and aerodynamic forces, surface tension, wave structures, ligament formation and bursting bubbles all contribute to the breakup process.

The PIV characterization of the air flow field shows an increasing velocity in the flow direction at the plane Z=0. This is attributed to boundary layer buildup on the walls.

Both PIV and PDA measurements show that small particles are more readily accelerated in the X direction by the air flow field, while larger droplets and ligament fractions will be injected further into the flow field (towards larger Y coordinates). A biased droplet size distribution will result. The droplet velocity field will also be biased with higher velocities at lower Y coordinates.

In the core region of the spray droplet velocities tend to decrease slightly due to the locally reduced aerodynamic loading, while outside the core droplet velocities are slightly elevated over the mean. Droplet average velocities goes from 21 m/s at plane 1 to 29 m/s at plane 5.

Averaged RMS velocities stays fairly constant at approximately 5 m/s throughout the test section. A slight increase in RMS values are seen at the spray core.

Droplet size and velocity distribution in the Y direction tend to even out towards plane 5.

5. ACKNOWLEDGEMENTS

We wish to thank Volvo Car Corporation, Vinnova, Fredrik Johansson and Ingjald Andreasson from the Department of Energy Sciences for kind assistance.

6. NOMENCLATURE

D	diameter of orifice	[mm]
	initial jet diameter	[mm]
	droplet diameter	[mm]
L/D	length/diameter of orifice	
q	liquid-to-air momentum flux ratio $\left(\frac{\rho_l \cdot u_l^2}{\rho_a \cdot u_a^2}\right)$	
SMD	Sauter Mean Diameter, D[3,2]	[μm]
U	velocity in X direction	[m/s]
ρ	density	[kg/m^3]
σ	surface tension	[N/m]
We	gas Weber number $\left(\frac{\rho_a \cdot U_{rel}^2 \cdot D}{\sigma}\right)$	
X, Y, Z	cartesian coordinates	[m]

Subscripts

a	air
l	liquid
rel	relative

7. REFERENCES

1. Gosh, S., Hunt, J., C., R., Spray Jets in a Cross-flow, J. Fluid Mech., Vol. 365, pp 109-136, 1998
2. Birouk, M, Azzopardi, B. J., Stäbler, T, Viscosity Effect on the Break-up of a Liquid Jet in a Cross Airflow, Ninth Intl. Conf. on Liquid Atomization and Spray Systems, Sorento, Italy, 2003
3. Rachner, M, Becker, J, Hassa, C, and Doerr, T, Modelling of the atomization of a plain liquid fuel jet in cross flow at gas turbine conditions, Elsevier, 2001.
4. Cavaliere, A., Ragucci R., Noviello C., Bending and break-up of a liquid jet in a high pressure airflow, Elsevier 2002
5. Johnson, J. N., Lubarsky, E., Zinn B. T., Experimental Investigation of Spray Dynamics Under Jet Engine Augmentor-Like Conditions, Proceedings of GT-2006-91112 ASME Turbo Expo 2006
6. Bayvel, L., Orzechovski, Z., Liquid Atomization, Taylor & Francis, ISBN 0-89116-959-8, 1993